**ORIGINAL PAPER**

# Physiologically-based pharmacokinetic model for pulmonary disposition of protein therapeutics in humans

Prabhas Jagdale[1] · Armin Sepp[2] · Dhaval K. Shah[1]

**Abstract**

Lung related disorders like COPD and Asthma, as well as various infectious diseases, form a major therapeutic area which would benefit from a predictive and adaptable mathematical model for describing pulmonary disposition of biological modalities. In this study we fill that gap by extending the cross-species two-pore physiologically-based pharmacokinetic (PBPK) platform with more detailed respiratory tract that includes the airways and alveolar space with epithelial lining fluid. We parameterize the paracellular and FcRn-facilitated exchange pathways between the epithelial lining fluid and lung interstitial space by building a mechanistic model for the exchange between the two. The optimized two-pore PBPK model described pulmonary exposure of several systemically dosed mAbs for which data is available and is also in agreement with the observed levels of endogenous IgG and albumin. The proposed framework can be used to assess pharmacokinetics of new lung-targeting biologic therapies and guide their dosing to achieve desired exposure at the pulmonary site-of-action.

## Introduction

The incidence of lung disorders has been on the rise since the past couple of decades. A majority of the respiratory diseases observed today can be attributed to tobacco smoke, indoor or outdoor air pollution, and genetics [1]. In the United States, in 1980 the risk of death due to chronic respiratory illness was about 41 deaths per 100,000 people. Since then, it has risen to about 53 deaths per 100,000 people in 2014, almost a 31% rise in death risk due to respiratory issues. The Forum of International Respiratory Societies has released a report, identifying asthma, chronic obstructive pulmonary disease (COPD), acute respiratory

infections, tuberculosis, and lung cancer as the top contributor to the global burden of respiratory diseases [2]; to which infectious diseases from common cold, influeza, tuberculosis and Covid-19 can be added too. About 65 million people suffer from COPD. The disorder kills 3 million people every year, making it the third leading cause of death worldwide. The CDC has estimated the total expenditure from 2011 to 2015 on treatment of Asthma and COPD was about $7 billion and $5 billion dollars, respectively [3]. Thus, pulmonary disorder is a major therapeutics area with intense research going on in the field.

In the past 25 years, the use of protein therapeutics has been rising steadily, with approximately one third of all drugs approved by the FDA being biologics such as monoclonal antibodies. As macromolecules have large interaction surfaces, they can display high-affinity binding and hence are uniquely suitable for competing with endogenous protein–protein interactions, albeit in extracellular space only. Unlike small molecule drugs, their breakdown products are naturally occurring amino acids which pose no toxicity risks, although pharmacological adverse effects

✉ Dhaval K. Shah
dshah4@buffalo.edu

1 Department of Pharmaceutical Sciences, School of Pharmacy and Pharmaceutical Sciences, The State University of New York at Buffalo, 455 Pharmacy Building, Buffalo, NY 14214-8033, USA

2 Simcyp Division, Certara UK Ltd, 1 Concourse Way, Level 2-Acero, Sheffield S1 2BJ, UK

remain a possibility [4]. The benefits provided by protein therapeutics outweigh the risks and a number of new drugs to treat pulmonary diseases, including COVID-19 have been biologics.

Lung delivery of biologics can be achieved through systemic or pulmonary dosing. Systemic intravenous or subcutaneous dosing is well established but involves delay before the drug reaches lung and alveolar space, with only a small fraction of the drug eventually reaching that space at concentration that is substantially lower than in plasma [5]. Inhalation, on the other hand, affords instant, frequent and high exposure throughout the respiratory tract, but faces distinct challenges of its own. The bioavailability of the pulmonary dose, as well as relative distribution along the respiratory tract, depend on the formulation, principally the size of the particle or droplet. In the case of solids or aerosol droplets with diameter in the range of 1–5 μm, as typical for nebulizers [6], around 70–80% of dose is retained overall but only about a third of that is deposited in the alveolar space [7]. The absorbed protein initially encounters the epithelial lining fluid (ELF), which is a thin layer of liquid of complex composition containing high levels of proteoglycans and surfactant proteins among others [8]. This is followed by the competing processes of size-dependent absorption into systemic circulation and non-specific degradation in situ. As a result, the systemic bioavailability for the locally administered dose declines from close to 100% for small molecules to almost 0% for large proteins like albumin and IgG. In the case of insulin, 10–20% bioavailability is accomplished following non-specific alveolar degradation with half-life around two hours [9, 10]. In addition, pulmonary administration of several other proteins such as Epo-Fc, INF-α etc. is actively being explored for systemic delivery [11, 12]. Despite the potential advantages, most of the approved new inhaled medicines have been small molecules over the past decades, with only a small number being biologics [13], which reflects the challenges involved in successful systemic delivery of proteins following pulmonary administration.

In order to facilitate the development of biologics for pulmonary disorders, following local or systemic administration, it is important to understand all the processes responsible for the disposition of biologics in the lung. Mathematical models that can describe the pharmacokinetics of biologics in the lung provide an opportunity to accomplish this goal in a thorough and quantitative manner. A number of compartmental, semi-mechanistic and physiologically-based pharmacokinetic (PBPK) models have been published in the past to describe pulmonary PK of small molecule drugs [14–17]. However, such models are lacking for biologics. Here we propose a novel model to describe the PK of protein therapeutics in the lung, based on the PBPK framework, which explicitly combines the information about the characteristics of the drugs and

targets with species-related physiological parameters. PBPK models take into account the organ-level transport processes and allows one to describe the local exposure at the site-of-action [18], which ultimately provide the link to any downstream pharmacology. PBPK models can also incorporate interactions with target(s) on cell surfaces and in solution, as well as micropinocytosis and subsequent recycling and transcytosis for proteins with FcRn-binding. In addition, PBPK models can be translated from one species to another with relative ease by changing the respective physiological parameters and rate constants. As such, PBPK models can serve as a cornerstone for model-informed drug discovery and development (MIDD), and can help improve clinical trial efficiency and optimize drug dosing recommendations.

In 2019, Sepp et al. [19] proposed a cross-species/cross-modalities platform two-pore PBPK model for biologics, built on the concept of platform PBPK model for monoclonal antibodies (mAbs) described by Shah and Betts [20], to capture plasma and tissue PK of different sized proteins. In the present study, we present an expansion of this approach to include a detailed model for the lungs, which captures processes involved in the disposition of proteins therapeutics in the alveolar pathway, upper and lower respiratory tract areas, including FcRn mediated transcytosis and paracellular exchange pathways. The involvement of transcytosis and paracellular transport across lung epithelium has been a topic of discussion for a long time. A number of in-vitro, in-vivo and ex-vivo studies conducted have shown that FcRn-transcytosis might be involved in transport of IgG and Fc-Fusion proteins across the lung epithelium [21–24]. As such, the presence of FcRn receptor in the upper and lower pathway including the alveolar epithelium [25, 26] presents the possibility that these airway regions could be involved in transport of IgGs and Fc-Fusion proteins across the pulmonary epithelium. Here we have used the PBPK model structure to further elucidate the role of FcRn in pulmonary disposition of protein therapeutics. While the PBPK model presented in this manuscript has been developed using systemically dosed mAb, and endogenous antibody and albumin data, it can also form the basis for describing pulmonary PK of other therapeutic proteins, endogenous or engineered, following local administration.

## Methods

### Experimental data for model building

We utilized data from several publications investigating the PK of monoclonal antibodies in Humans. Further, we used

data detailing endogenous IgG and endogenous Albumin levels in serum and bronchoalveolar lavage fluid samples.

Data for mAb levels in the epithelial lining fluid was obtained from a study by Magyarics et al. [27] The authors dosed subjects with ASN100 (Contains two fully human IgG1 mAbs, ASN-1 and ASN-2) at two different dose levels: 1800 mg and 4000 mg. Serum samples were collected and bronchoalveolar lavage (BAL) was collected to obtain ELF concentrations of subjects either on days 1 and 30, or on days 2 and 8. Consequently, concentrations of ASN-1 and ASN-2 in the serum and BAL samples were analyzed using ELISA [27]. In another study published by Deng et al. [28], authors investigated the disposition of MHAA4549A (a human anti-influenza IgG1 mAb) in upper airways ELF by quantifying Nasal Lavage Fluid (NLF). 60 subjects received an intravenous infusion of MHAA4549A at three single-dose levels (400, 1200 or 3600 mg). Serum samples for PK analysis were collected after infusion at the following time intervals: at 30 min and 4 h on day 1, day 2, 4, 8, 15, 57, 85, and 120 after the infusion. Nasal fluid using nasopharyngeal swabs were collected on days 1–8. Serum and nasal concentrations of MHAA4549A antibody were quantified by ELISA [28].

An additional dataset by Wollacott et al. [29] detailed nasal concentrations of intravenously infused mAb VIS410 (neutralizing monoclonal antibody against Influenza A). The subjects were dosed with 2, 5, 15, 30 and 50 mg/kg doses. Serum samples were collected from study subjects after infusion on days 1, 2, 3, 7, 14, 28, 56 and 120. Further, nasopharyngeal swabs were collected after infusion on days 1, 3, and 7 from 15, 30 and 50 mg/kg cohorts. Serum and Nasal samples were analyzed using ELISA [29].

Endogenous data for IgG and albumin was obtained from several sources to build the pulmonary PBPK model. In the study by Yoshida et al.[30] authors measured the endogenous IgG level in serum and in nasal lavage fluid (NLF) using Time-resolved fluorescence immunosorbent assay of antibodies and normalized the NLF concentrations using urea [30]. Another study by Merrill et al. [31] measured endogenous level of IgG in epithelial lining fluid via BAL. Urea normalized endogenous albumin levels in serum and BAL fluid samples were referenced from a study done by Wilson et al.[32]

## Platform PBPK model

The structure of the whole-body PBPK model with the expanded Lung compartment is described in Fig. 1. The model incorporates venous and arterial blood compartments, along with 14 other major tissues: lungs, lumped lymph nodes, heart, lumped gastrointestinal tract, liver, spleen, pancreas, muscle, skin, bone, brain, thymus,

adipose, and kidney. The 15th other compartment comprises of all other remaining tissues not explicitly mentioned in the model. All the tissues are connected anatomically via plasma and lymph flows, the lymphatic fluid is recirculated through the lymph nodes. All organs are divided into vascular, endosomal, and interstitial compartments as described in Fig. 2. The endosomal compartment contains the FcRn receptor that is responsible for recycling of IgG and albumin.

Each tissue has an inward plasma flow ($Q_{org}$) and outward flow of plasma ($Q_{org} - L_{org}$) and lymph ($L_{org}$). The IgG within the vascular compartment enters the tissue by two different processes. The first process describes the exchange of protein between vascular and interstitial compartment using a 2-pore paracellular process ($V2Pi_{tissue}$), which takes into account the heterogeneity in the size of paracellular pores, net ($L_{org}$) and isogravimetric ($L_{iso,org}$) lymph flow in the tissue for paracellular filtration, and the permeability surface area product ($PS_{org}$) for diffusion [19]. Second, all soluble proteins in the vascular space are assumed to be taken up into the endosomal space through pinocytosis ($K_{up}$), where the proteins could form a complex with FcRn receptor and be recycled ($K_{rec}$) back to vascular or interstitial space [19]. Unbound IgG in the endosomal space was assumed to degrade by a first-order degradation process ($K_{deg}$). Once the free IgG reaches the interstitial space, it was assumed to be cleared by lymphatic flow, where the reflection coefficient ($\sigma_i$) was used to characterize the resistance to the convective flow of proteins. Since the final PBPK model was used to capture the PK of three different mAbs together, any subtle differences between systemic PK of mAbs were characterized using a non-specific clearance parameter from the vascular space ($kdegV$).

The physiological parameters related to the tissue volumes and fluid flows were obtained from Shah and Betts 2012 [20], and are provided in Table 1. The description of the parameters used in the platform model are given in Table 2. For interstitial volumes, it was assumed that only 50% of the total interstitial volume is available for large molecular weight species like albumin and IgG [33]. The endosomal volume was set to 0.5% of the total tissue volume [34]. Fraction (FR) of FcRn bound antibody recycled to the vascular space was set to 0.715 [34, 35]. FcRn monovalent affinity ($Kd_{FcRn}$) for IgG was set to 998 nM and the respective avidity coefficient for IgG was set to 10, since an IgG can engage two FcRn molecules at the same time [36]. Two pore extravasation parameters, lymph to plasma ratio for each individual organ, large pore and small pore radius, tissue specific relative large pore and small pore hydraulic conductance, and reflection coefficients were adopted from the publication by Sepp et al.

**Fig. 1** Schematic of the whole body PBPK model for protein therapeutic disposition. Rectangular boxes represent tissue compartments and solid and dashed arrows represent plasma and lymph flow, respectively
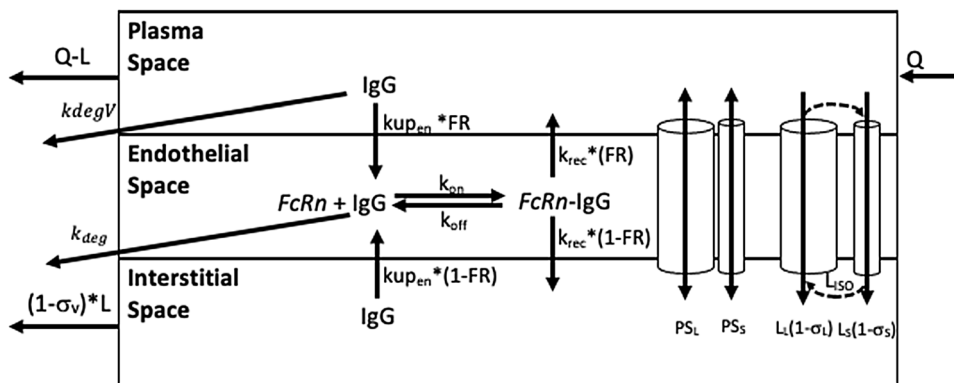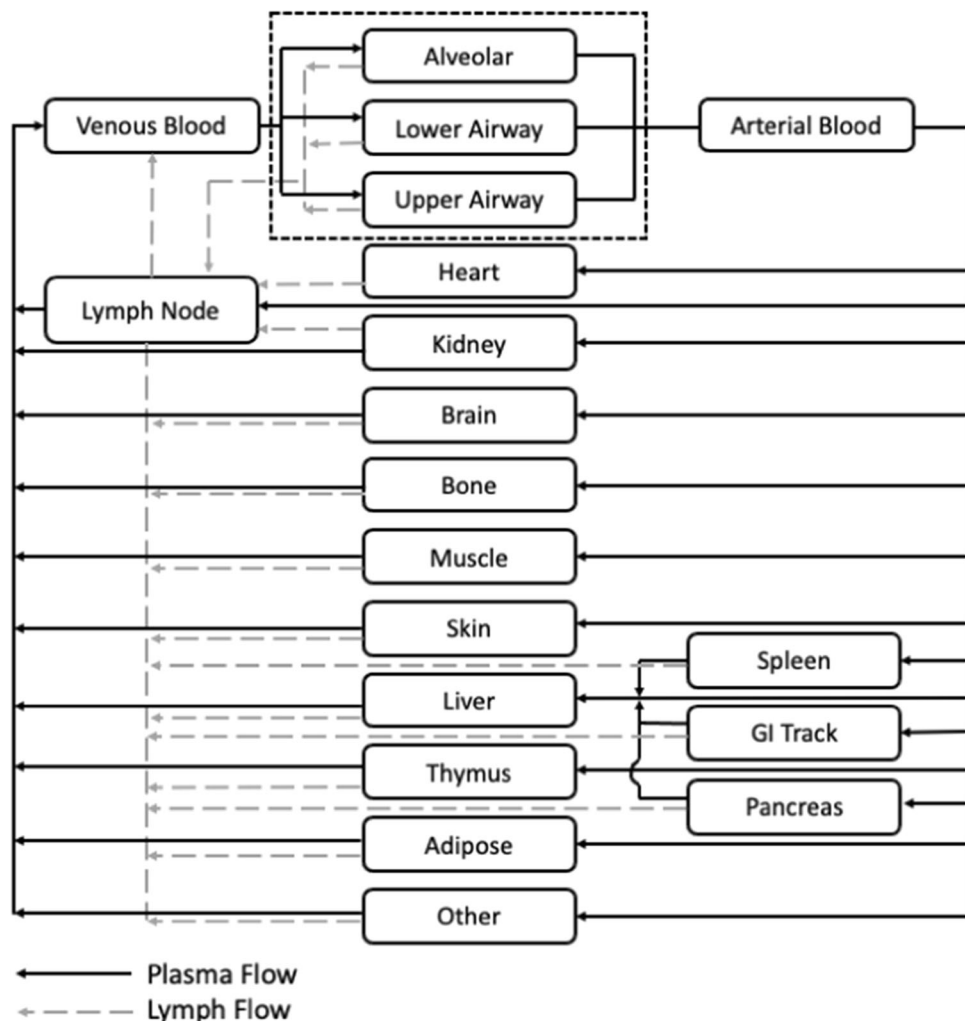


**Fig. 2** Schematic of generic tissue level structure of the PBPK model. Each tissue compartment except, arterial and venous blood, lungs, kidney and brain are further divided in to Plasma space, endothelial endosomal space and interstitial space. Each tissue has an inward plasma flow ($Q_{org}$) and outward flow of plasma ($Q_{org} - L_{org}$) and lymph ($L_{org}$). The IgG in plasma space can enter the tissue by either pinocytosis uptake or through 2-pore paracellular transport between plasma and interstitial space. The endosomal space contains FcRn receptor which is responsible for FcRn mediated transcytosis. For detailed description of the drug disposition process please refer to "Platform PBPK Model" in sub-section in "methods" section

**Table 1** Physiological parameters used for human PBPK model

|  | Total volume (L) | Plasma volume (L) | Interstitial volume (L) | Endosomal volume (L) | Cellular volume (L) | Plasma flow (L/h) |
|---|---|---|---|---|---|---|
| Lung | 2.29401 | 0.649011 | 0.188568 | 0.005 | 0.595 | 181.9125 |
| Heart | 0.34151 | 0.012887 | 0.0488 | 0.001705 | 0.267 | 7.7517 |
| Kidney | 0.33157 | 0.017963 | 0.0498 | 0.00166 | 0.247 | 36.4023 |
| Muscle | 30.07844 | 0.649011 | 3.91 | 0.15039 | 24.815 | 33.4686 |
| Skin | 3.408 | 0.126132 | 1.125 | 0.01704 | 2.035 | 11.6259 |
| Brain | 1.31492 | 0.028897 | 0.236686 | 0.00725 | 1.124 | 21.4533 |
| Adipose | 13.46515 | 0.165963 | 2.289 | 0.067325 | 10.84 | 11.2332 |
| Thymus | 0.00639 | 0.000391 | 0.00109 | 3.21E-05 | 0.00465 | 0.3531 |
| GIT | 2.14065 | 0.017963 | 0.349068 | 0.001925 | 0.305 | 26.9973 |
| Spleen | 0.22152 | 0.026554 | 0.0443 | 0.001105 | 0.127 | 6.3426 |
| Pancreas | 0.10366 | 0.003905 | 0.018 | 0.00052 | 0.0747 | 3.0558 |
| Liver | 2.14278 | 0.121446 | 0.429 | 0.010715 | 1.371 | 13.2099 |
| Bone | 10.16436 | 0.142142 | 1.891 | 0.050825 | 7.817 | 2.5905 |
| Ly. node | 0.27406 | 0.011154 | 0.093898 | 0.00137 | 0.274 | 3.63 |
| Other | 2.797647 | 0.012496 | 0.443625 | 0.02426 | 3.626 | 3.7983 |
| Arterial | 0.957667 | 0.574621 | … | … | … | … |
| Venous | 0.957667 | 0.574621 | … | … | … | … |

[19] Of note, these parameter values are assumed to be conserved across species. The IgG to FcRn association constant ($Kon_{FcRn}$) was set to 1E9 M$^{-1}$ h$^{-1}$ and dissociation constant ($Koff_{FcRn}$) was calculated as the product of association constant and FcRn monovalent affinity to IgG ($Kon_{FcRn}*Kd_{FcRn}$). The uptake clearance rate by endothelial cells ($K_{up}$), FcRn recycling rate of endothelial and epithelial cells ($K_{rec}$, $K_{recEpi}$), endosomal degradation rate ($K_{deg}$), and FcRn concentrations in endothelial and epithelial cells were set to 0.1 h$^{-1}$, 11.7 h$^{-1}$, 152.8 h$^{-1}$ and 9.1 E-6 M$^{-1}$ respectively [19, 37]. Equations for the whole-body platform PBPK model are provided below.

### Arterial compartment

$$\frac{d(C_{arterial})}{dt} = \Big( Q_{lu_{al}} * C_{lu_{alva}} + Q_{lu_{LA}} * C_{lu_{LAva}} + Q_{lu_{UA}} * C_{lu_{UAva}}$$
$$- kdegV * C_{arterial} * V_{arterial} - (Q_{he} + Q_{mu}$$
$$+ Q_{sk} + Q_{ad} + Q_{bo} + Q_{br} + Q_{th} + Q_{ki} + Q_{li}$$
$$+ Q_{gi} + Q_{pa} + Q_{sp} + Q_{ln} + Q_{ot}) * C_{arterial} \Big)$$
$$* \left( \frac{1}{V_{arterial}} \right)$$

(1)

### Venous compartment

$$\frac{d(C_{venous})}{dt} = \Big( -(Q_{lu_{al}} + L_{lu_{al}}) * C_{venous} - (Q_{lu_{LA}} + L_{lu_{LA}})$$
$$* C_{venous} - (Q_{lu_{UA}} + L_{lu_{UA}}) * C_{venous} - kdegV$$
$$* C_{venous} * V_{venous} + (Q_{he} - L_{he}) * C_{he_{va}}$$
$$+ (Q_{mu} - L_{mu}) * C_{mu_{va}} + (Q_{sk} - L_{sk}) * C_{sk_{va}}$$
$$+ (Q_{ad} - L_{ad}) * C_{ad_{va}} + (Q_{bo} - L_{bo}) * C_{bo_{va}}$$
$$+ (Q_{br} - L_{br}) * C_{br_{va}} + (Q_{th} - L_{th}) * C_{th_{va}}$$
$$+ (Q_{ki} - L_{ki}) * C_{ki_{va}} + ((Q_{li} - L_{li}) + (Q_{gi} - L_{gi})$$
$$+ (Q_{pa} - L_{pa}) + (Q_{sp} - L_{sp})) * C_{li_{va}} + (Q_{ln} - L_{ln})$$
$$* C_{ln_{va}} + (Q_{ot} - L_{ot}) * C_{ot_{va}} + (L_{lu_{al}} + L_{lu_{LA}} + L_{lu_{UA}}$$
$$+ L_{he} + L_{mu} + L_{sk} + L_{ad} + L_{bo} + L_{br} + L_{th} + L_{ki} + L_{li}$$
$$+ L_{gi} + L_{pa} + L_{sp} + L_{ln} + L_{ot}) * C_{ln_{in}} \Big) * \left( \frac{1}{V_{venous}} \right)$$

(2)

**Table 2** Glossary of parameters used in the PBPK model

| Parameter | Units | Definition |
|---|---|---|
| $Q_i$ | $L/h$ | Plasma flow to tissue "$i$" |
| $L_i$ | $L/h$ | Lymph flow from the tissue "$i$" |
| $V_{arterial}, V_{venous}, V_{LN}$ | $L$ | Volumes of the arterial venous, and lymph node compartments |
| $V_{i_{va}}, V_{i_E}, V_{i_{IS}}$ | $L$ | Volumes of the vascular, endosomal, and interstitial compartments for the tissue "$i$" |
| $C_{arterial}, C_{venous}, C_{LN}$ | $M$ | Concentrations in the arterial venous, and lymph node compartments |
| $C_{i_{va}}, C_{i_{EU}}, C_{i_{EB}}, C_{i_{IS}},$ | $nM$ | Concentrations in the vascular, endosomal (Unbound and Bound) and interstitial for the tissue "$i$" |
| $kdegV$ | $1/h$ | Non-specific vascular rate of clearance of antibodies |
| $FcRn$ | $M$ | Concentration of FcRn in the endosomal space |
| $\sigma_{i_{IS}}$ | – | Lymph reflection coefficient |
| $Kon_{FcRn}$ | $1/M/h$ | Association rate constants between mAb and FcRn |
| $Koff_{FcRn}$ | $1/h$ | Dissociation rate constants between mAb and FcRn |
| $FR$ | – | Fraction of FcRn bound mAb that recycles to the vascular space |
| $K_{up}$ | $1/h$ | Rate of pinocytosis and exocytosis per unit endosomal space of the vascular endothelium |
| $K_{deg}$ | $1/h$ | First-order degradation rate constant of FcRn-unbound mAb in the endosomal space |
| $PS_i$ | $mole/h$ | 2 pore paracellular transport of mAb between Vascular and Interstitial compartments |
| $K_{rec}$ | $1/h$ | Rate of recycling of FcRn receptor |
| $V_{lu_{xva}}, V_{lu_{xE}}, V_{lu_{xIS}}, V_{lu_{xEpi}}, V_{lu_{xELF}}$ | $L$ | Volumes of the vascular, Endothelial, interstitial, Epithelial and Epithelial Lining Fluid compartments of alveolar pathway, lower airway and upper airway |
| $C_{lu_{xal}}, C_{lu_{xEU}}, C_{lu_{xEB}}, C_{lu_{xIS}}, C_{lu_{xEpiU}}, C_{lu_{xEpiB}}, C_{lu_{xELF}}$ | $M$ | Concentrations in the vascular, endosomal (Unbound and Bound), interstitial, epithelial (Unbound and Bound) and ELF compartments of alveolar pathway, lower airway and upper airway |
| $Q_{lu_{al}}, Q_{lu_{LA}}, Q_{lu_{UA}}$ | $L/h$ | Plasma flow to vascular compartments of alveolar pathway, lower airway and upper airway |
| $L_{lu_{al}}, L_{lu_{LA}}, L_{lu_{UA}}$ | $L/h$ | Lymph flow from the alveolar pathway, lower airway and upper airway |
| $FcRn_{lu_{xE}}, FcRn_{lu_{xEpi}}$ | $M$ | FcRn concentration of endosomal and epithelial compartments of alveolar pathway, lower airway and upper airway |
| $K_{upEpi}$ | $1/h$ | Rate of pinocytosis and exocytosis per unit endosomal space of the epithelium |
| $V2Pi_{lu_{al}}, V2Pi_{lu_{LA}}, V2Pi_{lu_{UA}}$ | $L/h$ | 2 pore paracellular transport of mAb between Vascular and Interstitial compartments of alveolar pathway, lower airway and upper airway |
| $PS_{drug_{al}}, PS_{drug_{LA}}, PS_{drug_{UA}}$ | $L/h$ | Permeability surface area products from drugs across epithelial lining fluid and interstitial space |
| $Kabs_{al}, Kabs_{LA}, Kabs_{UA}$ | $1/h$ | Rate of paracellular transport between epithelial lining fluid and interstitial space |
| $K_{deposition}$ | $1/h$ | Rate of deposition of drug from airway to ELF |
| $K_{recEpi}$ | $1/h$ | Rate of recycling of FcRn receptor in epithelial endosomal space |
| $K_{deg_{al}}, K_{deg_{LA}}, K_{deg_{UA}}$ | $1/h$ | First-order degradation rate constant of protein in the ELF space of alveolar pathway, lower airway and upper airway |
| $F_{lu_{drug}}$ | – | Fraction of drug absorbed from ELF into Interstitial space |
| $f_{Q_{al}}, f_{Q_{LA}}, f_{Q_{UA}}$ | – | Fraction of pulmonary blood flow going to the alveolar, lower airway and upper airway pathways |
| $f_{lu_{lymph}}$ | – | Fraction of lung plasma flow redirected to lymph flow of lungs |
| $FR_{Epi}$ | – | Fraction of FcRn bound mAb in epithelial endosomal space that recycles to the ELF space |
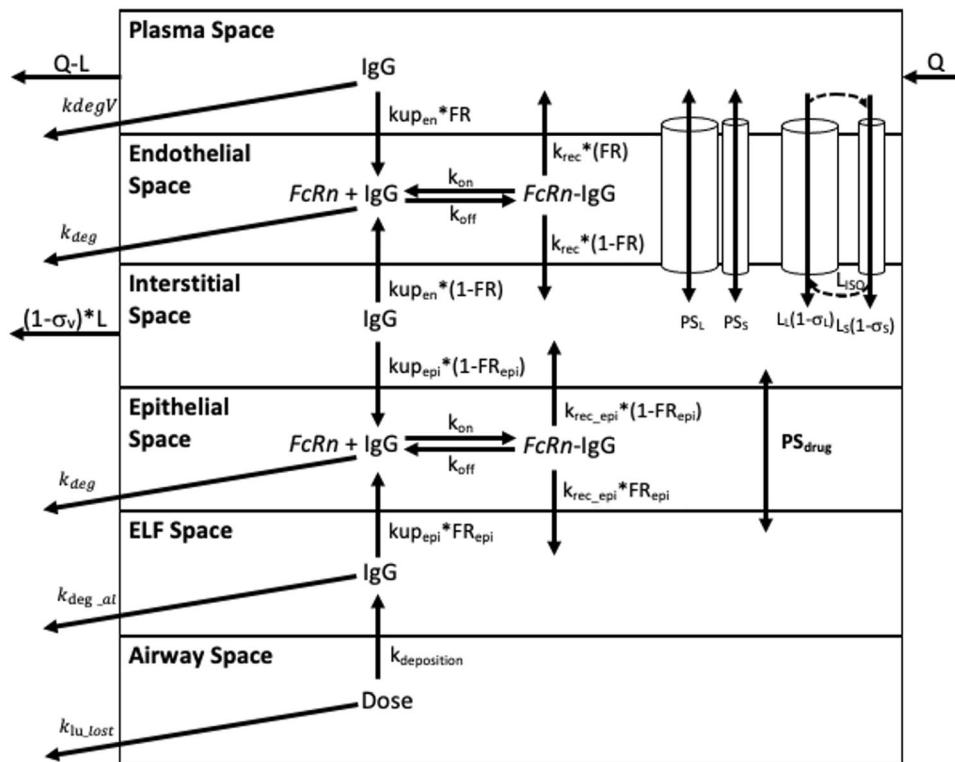
**Fig. 3** Schematic of the physiologically based lung compartment. Alveolar space is shown for demonstration, but the upper airway and lower airway pathways follow the same schematic as the alveolar pathway. The sub-compartments are connected in an anatomical manner including blood, lymph, 2-pore paracellular flow between vascular and interstitial space, permeability surface area product of drugs across ELF Space. The Endothelial and Epithelial space implies the endosomal space in these compartments and accounts for FcRn

mediated transcytosis and endosomal uptake through micropinocytosis ($Kup_{en}(= Kup) and Kup_{epi}$). The plasma, endothelial and interstitial space mimics the process as in the generic tissue structure of the model. The paracellular transport across Interstitial and ELF space is reflected by $PS_{drug}$ process. The drug in the airways is deposited on the epithelial lining fluid, $K_{deposition}$ is the rate of deposition and $K_{lu_{lost}}$ reflects the rate at which undeposited drug is disposed from the airway space

## Generic tissue compartment

Vascular space

$$\frac{d(C_{tissue_{va}})}{dt} = \left( Q_{tissue} * C_{arterial} - (Q_{tissue} - L_{tissue}) \right.$$
$$* C_{tissue_{va}} - K_{up} * FR * C_{tissue_{va}} * V_{tissue_E}$$
$$- V2Pi_{tissue} * (C_{tissue_{va}} - C_{tissue_{IS}}) - kdegV$$
$$* C_{tissue_{va}} * V_{tissue_{va}} + (k_{rec} * V_{tissue_E} * FR * C_{tissue_{EB}}) \big)$$
$$* \left( \frac{1}{V_{tissue_{va}}} \right)$$

$$(3)$$

Endosomal space protein unbound to FcRn

$$\frac{d(C_{Tissue_{EU}})}{dt} = K_{up} * (FR * C_{tissue_{va}} + (1 - FR) * C_{tissue_{IS}})$$
$$- kon_{FcRn} * C_{tissue_{EU}} * FcRn_{tissue_E}$$
$$+ Koff_{FcRn} * C_{tissue_{EB}} - K_{deg} * C_{tissue_{EU}}$$

$$(4)$$

Endosomal space protein bound to FcRn

$$\frac{d(C_{tissue_{EB}})}{dt} = kon_{FcRn} * C_{tissue_{EB}} * FcRn_{tissue_E} - Koff_{FcRn}$$
$$* C_{tissue_{EB}} - k_{rec} * C_{tissue_{EB}}$$

$$(5)$$

Endosomal space FcRn

$$\frac{d(FcRn_{tissue_E})}{dt} = k_{rec} * C_{tissue_{EB}} - kon_{FcRn} * C_{tissue_{EU}}$$
$$* FcRn_{tissue_E} + koff_{FcRn} * C_{tissue_{EB}}$$

$$(6)$$

Interstitial space

$$\frac{d(C_{tissue_{IS}})}{dt} = (k_{rec} * (1 - FR) * C_{tissue_{EB}} * V_{tissue_E} - K_{up}$$
$$* FR * C_{tissue_{IS}} * V_{tissue_E} + V2Pi_{tissue}$$
$$* (C_{tissue_{va}} - C_{tissue_{IS}}) - L_{tissue}$$
$$* (1 - ISRC_{tissue}) * C_{tissue_{IS}}) * \left( \frac{1}{V_{tissue_{IS}}} \right)$$

$$(7)$$

where, $ISRC_{tissue}$ is the lymphatic reflection coefficient for the tissue.

In addition, the kidney, brain and lung compartments carry further organ-specific modifications. The Kidneys describe protein size-dependent glomerular filtration and contain an additional lumped compartment containing the Bowman's capsule and loops of Henle (BCLH). The brain interstitial space is supplemented with cerebrospinal fluid flow that traverses the vascular barrier from capillaries into interstitial space, from where it empties into the central circulation, as in the previous model published by Sepp et al. [19]

## The lung compartment

We have expanded the previously published model [19] by adding a novel detailed lung compartment to include the upper and lower airways of the respiratory tract. The tissue structure for the compartment is presented in Fig. 3. The lung compartment has been modified to include the upper airway, the lower airway and the alveolar pathway. Physiologically the upper airways, which account for the trachea and nasal epithelium are not a part of the lungs and have a separate arterial blood supply, but for the purpose of model simplification we have considered it to be a part of the pulmonary region. All three lung compartments share the same structure and are divided into 6 sub-compartments: vascular, endothelial endosomal, interstitial,

**Table 3** Physiological parameters for the lung component of the PBPK model

| Parameter | Value | Source |
|---|---|---|
| $Q_{lu_{al}}$(L/h) | $Q_{lu} * f_{al_{drug}}$ | Calculated |
| $Q_{lu_{LA}}$(L/h) | $Q_{lu} * f_{LA_{drug}}$ | Calculated |
| $Q_{lu_{UA}}$(L/h) | $Q_{lu} * f_{UA_{drug}}$ | Calculated |
| $L_{lu_{al}}$(L/h) | $Q_{lu_{al}} * f_{lu_{lymph}}$ | Calculated |
| $L_{lu_{LA}}$(L/h) | $Q_{lu_{LA}} * f_{lu_{lymph}}$ | Calculated |
| $L_{lu_{UA}}$(L/h) | $Q_{lu_{UA}} * f_{lu_{lymph}}$ | Calculated |
| $f_{lu_{lymph}}$ | 6.44E-6 | [19] |
| $Kabs_{al}$(1/h) | | Equation (8) |
| $Kabs_{LA}$(1/h) | | Equation (8) |
| $Kabs_{UA}$(1/h) | | Estimated |
| $K_{recEpi}$(1/h) | 11.7 | [19] |
| $F_{lu_{drug}}$ | | Equation (10) |
| $K_{upEpi}$(1/h) | – | Estimated |

epithelial endosomal, epithelial lining fluid (ELF) and airway space. The physiological parameters used for lung compartment are provided in Table 3. The plasma flow to lungs has been divided amongst alveolar pathway, upper airways, and lower airways as 92.5%, 5% and 2.5%, respectively [15]. The volumes of different sub-compartments (vascular, endothelial, interstitial, and epithelial) of each of the lung compartments were calculated as a percentage of the total volume of each lung compartment. 83.34% of the lung volume was assigned to alveolar pathway, and the remaining 16.66% was equally split amongst the upper and lower airways [15]. Volume of epithelial lining fluid compartment for the three pathways was calculated as the product of the average thickness of the epithelial lining fluid and the reported surface area of the compartments [38–40]. The volumes of sub-compartments of the Lung are mentioned in Table 4.

Vascular and interstitial spaces in the sub-compartments of the lung are treated similar to other tissues, with inward flow of plasma ($Q_{lu_x} + L_{lu_x}$) and outward plasma ($Q_{lu_x}$) and lymph flow ($L_{lu_x}$) through the lymph nodes. The soluble protein in the vascular space can be taken up into the tissue by two processes: (1) 2-pore paracellular transport into interstitial space, and (2) pinocytosis ($K_{up}$) into the endothelial endosomal compartment. Once in the endothelial endosomal space, the protein can form a reversible complex with FcRn and can be recycled back to extracellular space, while the free protein is degraded by first-order non-specific endosomal degradation process ($K_{deg}$) as described for other tissues. Similar principle applies to the epithelial endosomal space, except that the respective surrounding extracellular spaces are interstitial space and ELF, and we postulate the paracellular transport to be diffusion-driven using protein size-dependent permeability-surface area product ($PS_{drug_x}$). Soluble protein in the ELF is subjected to first order enzymatic degradation ($K_{deg_x}$), which is calculated from Eq. 11.

While the present model mainly deals with systemically administered exogenous proteins and also, endogenous proteins, in order to make this platform amenable for local administration, it was assumed that proteins in the airway space enter ELF via a first order deposition rate constant ($K_{deposition}$), and the fraction of protein deposited can be adjusted between 0 and 1 based on the nature of the protein and the formulation. The Fraction of drug absorbed from the ELF ($F_{lu_{drug}}$) into systemic circulation in the alveolar and Lower Airway pathway is calculated from Eq. 10, derived from the data published by Sakagami et al. [9] (Fig. 4b). The permeability-surface area product ($PS_{drug_x}$) which describes the exchange between the lung interstitium and ELF is calculated using Eq. 9, where the rate of absorption ($K_{abs_X}$) from ELF into interstitial space for

**Table 4** Physiological parameters for tissue sub-compartments of the Lung compartment

| | Plasma volume (L) | Interstitial volume (L) | Endothelial endosomal volume (L) | Epithelial endosomal volume (L) | Epithelial lining fluid volume (L) |
|---|---|---|---|---|---|
| Alveolar | 0.54084 | 0.1574 | 0.0042 | 0.00248 | 0.0208 |
| Lower airway | 0.054084 | 0.01574 | 0.0004 | 0.000248 | 0.00208 |
| Upper airway | 0.005408 | 0.01574 | 0.0004 | 0.000248 | 0.0002 |
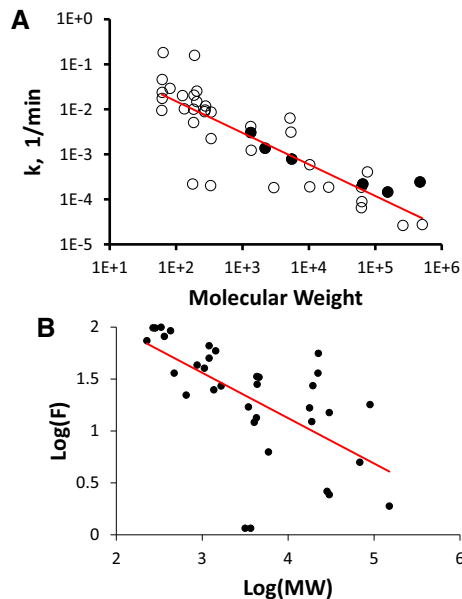


**Fig. 4 A** Effect of size on alveolar clearance of the proteins [22]. This relation was used to derive an empirical relation between size of protein and $Kabs_{al}$. **B** Log of percentage bioavailability as a function of log of protein size [9]. This was used to derive a mathematical relation between size and fraction of alveolar drug absorbed ($F_{al_{drug}}$)

## Lung sub-compartment related parameter equations used in the model

$$K_{abs_{al}} = K_{abs_{LA}} = 10^{-0.2 - 0.8 LOG(MW)} \tag{8}$$

$$PS_{drug_{al}} = K_{abs_{al}} * V_{lu_{al_{ELF}}} * (C_{lu_{al_{ELF}}} - C_{lu_{al_{IS}}}) \tag{9}$$

$$F_{lu_{Drug}} = 10^{(1 - 0.47 LOG(MW))} \tag{10}$$

$$K_{\deg_{al}} = Kabs_{al} * \left( \frac{1}{F_{lu_{Drug}}} - 1 \right) \tag{11}$$

$$Q_{lu_x} = Q_{lu} * f_{Q_x} \tag{12}$$

$$L_{lu_x} = Q_{lu_x} * f_{lu_{lymph}} \tag{13}$$

Above, subscript x denotes upper airways, lower airways or alveolar compartments.

Vascular space

$$
\begin{aligned}
\frac{d\left(C_{lu_{al_{va}}}\right)}{dt} = & \Big( (Q_{lu_{al}} + L_{lu_{al}}) * C_{venous} - Q_{lu_{al}} * C_{lu_{al_{va}}} \\
& - K_{up} * FR * C_{lu_{al_{va}}} * V_{lu_{al_E}} - V2Pi_{lu_{al}} \\
& * (C_{lu_{al_{va}}} - C_{lu_{al_{IS}}}) - kdegV * C_{lu_{al_{va}}} * V_{lu_{al_{va}}} \\
& + (k_{rec} * V_{lu_{al_E}} * FR * C_{lu_{al_{EB}}}) \Big) * \left( \frac{1}{V_{lu_{al_{va}}}} \right)
\end{aligned}
\tag{14}
$$

Endothelial endosomal space protein unbound to FcRn

$$
\begin{aligned}
\frac{d\left(C_{lu_{al_{EU}}}\right)}{dt} = & \big( K_{up} * (FR * C_{lu_{al_{va}}} + (1 - FR) * C_{lu_{al_{in}}}) \\
& - kon_{FcRn} * C_{lu_{al_{EU}}} * FcRn_{lu_{al_E}} + Koff_{FcRn} \\
& * C_{lu_{al_{EB}}} - K_{deg} * C_{lu_{al_{EU}}} \big)
\end{aligned}
\tag{15}
$$

Endothelial endosomal space protein bound to FcRn

$$
\begin{aligned}
\frac{d\left(C_{lu_{al_{EB}}}\right)}{dt} = & kon_{FcRn} * C_{lu_{al_{EU}}} * FcRn_{lu_{al_E}} - Koff_{FcRn} \\
& * C_{lu_{al_{EB}}} - k_{rec} * C_{lu_{al_{EB}}}
\end{aligned}
\tag{16}
$$

Endosomal space FcRn

alveolar and lower airways is calculated from Eq. 8 derived from the data published by Hastings et al.[22] (Fig. 4a). Non-specific degradation rate constant of proteins ($K_{\deg_X}$) in ELF is derived from Eq. 11 and is relatively independent of protein size with half-life $\sim$ 2–9 h in the alveolar and lower airway compartments. Below are the equations used to model the lung compartment.

$$\frac{d\left(FcRn_{lu_{al_E}}\right)}{dt} = k_{rec} * C_{lu_{al_{EB}}} - kon_{FcRn} * C_{lu_{al_{EU}}} * FcRn_{lu_{al_E}} + koff_{FcRn} * C_{lu_{al_{EB}}}$$

(17)

Interstitial space

$$\frac{d\left(C_{lu_{al_{IS}}}\right)}{dt} = (k_{rec} * (1 - FR) * C_{lu_{al_{EB}}} * V_{lu_{al_E}} - K_{up} * (1 - FR) * C_{lu_{al_{IS}}} * V_{lu_{al_E}} + V2Pi_{lu_{al}} * (C_{lu_{al_{va}}} - C_{lu_{al_{IS}}}) + k_{recEpi} * (1 - FR_{Epi}) * C_{lu_{al_{EpiB}}} * V_{lu_{al_{Epi}}} - K_{upEpi} * (1 - FR_{Epi}) * C_{lu_{al_{IS}}} * V_{lu_{al_{Epi}}} + PS_{drug_{al}} - L_{lu_{al}} * (1 - ISRC_{lu}) * C_{lu_{al_{IS}}}) * (\frac{1}{V_{lu_{al_{IS}}}})$$

(18)

Epithelial endosomal space protein unbound to FcRn

$$\frac{d\left(C_{lu_{al_{EpiU}}}\right)}{dt} = (K_{upEpi} * (FR_{Epi} * C_{lu_{al_{ELF}}} + (1 - FR_{Epi}) * C_{lu_{al_{in}}}) - kon_{FcRn} * C_{lu_{al_{EpiU}}} * FcRn_{lu_{al_{Epi}}} + Koff_{FcRn} * C_{lu_{al_{EpiB}}} - K_{deg} * C_{lu_{al_{EpiU}}})$$

(19)

Epithelial endosomal space protein bound to FcRn

$$\frac{d\left(C_{lu_{al_{EpiB}}}\right)}{dt} = kon_{FcRn} * C_{lu_{al_{EpiU}}} * FcRn_{lu_{al_{Epi}}} - Koff_{FcRn} * C_{lu_{al_{EpiB}}} - k_{recEpi} * C_{lu_{al_{EpiB}}}$$

(20)

Epithelial Endosomal Space FcRn

$$\frac{d\left(FcRn_{lu_{al_{Epi}}}\right)}{dt} = k_{recEpi} * C_{lu_{al_{EpiB}}} - kon_{FcRn} * C_{lu_{al_{EpiU}}} * FcRn_{lu_{al_{Epi}}} + koff_{FcRn} * C_{lu_{al_{EpiB}}}$$

(21)

ELF space

$$\frac{d\left(C_{lu_{al_{ELF}}}\right)}{dt} = (K_{deposition} * C_{lu_{al_{air}}} * V_{lu_{al_{ELF}}} + K_{recEpi} * V_{lu_{al_{Epi}}} * FR_{epi} * C_{lu_{al_{EpiB}}} - K_{upEpi} * (FR_{Epi}) * C_{lu_{al_{ELF}}} * V_{lu_{al_{Epi}}} - PS_{drug_{al}} - K_{deg} * C_{lu_{al_{ELF}}} * V_{lu_{al_{ELF}}}) * (\frac{1}{V_{lu_{al_{ELF}}}}).$$

(22)

## Parameter estimation and model simulation

The PBPK model was assembled using a Matlab script PBPKassembler [19]. Model fitting and simulations were carried out in SimBiology/Matlab version R2019b (Math-Works, Inc., Natick Massachusetts, USA 2019).

The plasma PK of the three antibodies (ASN1, ASN2 and MHAA) was used for estimation of parameters for ELF PK. The usual half-life of IgG1 is estimated to be around 21 days, but the halflife of VIS410 mAb had significant deviation from this (half life $\sim$ 12 days). Hence, this data was not used for estimating Pulmonary PK parameters. Nontheless, after adjusting the plasma PK, the data was used as an validation dataset. Since, each mAb has some deviations due to possible non-specific degradation or non-specific binding the Plamsa PK of each mAb was first captured by estimating a non-specific clearance term ($kdegV_x$) for each antibody. Once the plasma PK was captured accurately, two model parameters were estimated by simultaneously fitting three datasets for the mAbs listed above: (1) the rate of pinocytosis uptake ($K_{upEpi}$) for lung epithelial cells, and (2) the rate of absorption ($Kabs_{UA}$) from ELF to interstitial space for upper airway compartment. For simulating endogenous IgG and albumin levels in pulmonary tissues a synthesis rate was introduced in plasma while keeping all other parameters to their default values. The synthesis rate was fixed to achieve IgG plasma concentration levels of 9.5 g/L and 50 g/L for albumin [31, 32].

The performance of the platform PBPK model was evaluated by simulating the PK of mAbs in the ELF compartments of lower and upper airways after intravenous administration of antibodies. To check the predictive capability of the model we calculated the symmetric mean absolute percentage error (SMAPE) (Eq. 23) between the AUC ($AUC_{0-t} was used to calculate SMAPE$) of simulated PK profile ($AUC_{sim}$) and the AUC of observed PK profiles for indicated mAbs ($AUC_{obs}$). SMAPE value of 33% would suggest a twofold prediction error.

$$SMAPE = \frac{|AUC_{sim} - AUC_{obs}|}{\frac{1}{2}(|AUC_{sim}| + |AUC_{obs}|)} * 100\%$$

(23)

## Sensitivity analysis

As the lung compartment was expanded to include the lower airway and upper airway pathway, there were some parameters that needed to be estimated. It is possible that there are differences in the pinocytosis uptake and FcRn expressions levels of epithelial cells as compared to endosomal cells. Similarly, the thickness of epithelial lining fluid and also the mucus membrane decreases as we

move from the upper airways to alveolar pathway. Hence, the rate of absorption of protein from the ELF space to interstitial space would vary in these pathways as compared to alveolar pathway.

Thus, in order to identify parameters that have larger effect on model performance, a local sensitivity analysis was performed on the final model and parameters to assess the sensitivity of model parameters on the ELF concentration in upper and lower airways. The analysis was performed on four parameters: (1) the pinocytosis uptake by lung epithelial cells ($K_{upEpi}$),(2) FcRn endosomal concentration in lung epithelial cells ($FcRn_{epi}$), (3) rate of absorption from ELF in lower airway ($Kabs_{LA}$), and (4) rate of absorption from ELF in upper airway ($Kabs_{UA}$). For local sensitivity analysis area under the ELF concentration vs. time curve (AUC) ($AUC_{0-t}$) was chosen as the relevant model output to represent drug exposure. The percentage change in AUCs with $\pm 50\%$ alteration in model parameters was evaluated. [20]

$$\%Change = \frac{AUC_{SIM} - AUC_{\pm 50\%}}{AUC_{SIM}} * 100 \qquad (24)$$

$AUC_{SIM}$ refers to the AUC obtained with optimized set of parameters and $AUC_{\pm 50\%}$ refers to the AUC obtained by increasing and decreasing the model parameter value by 50%.

## Results

### Plasma PK fitting

As shown in Fig. 5, following the estimation of vascular degradation parameter $kdegV_x$ for antibodies ASN1, ANS2 and MHAA, the model was able to capture plasma PK of all the mAbs reasonably well. The estimated parameter values for $kdegV_{ASN1}, kdegV_{ASN2}, kdegV_{MHAA}$ are shown in Table 5.

### Lung parameter estimation

As outlined in the methods section, 2 studies administered ASN1 and ASN2 antibodies intravenously to subjects and determined antibody PK in the lower airway ELF by broncho alveolar lavage. In the study done by Deng et al. different doses of MHAA4549A were intravenously administered to subjects and concentration levels in upper airway ELF were measured. These three datasets were fitted simultaneously to estimate two parameters: (1) the pinocytosis uptake rate of lung epithelial cells ($K_{upEpi}$), and (2) the rate of upper airway absorption ($Kabs_{UA}$). As shown in Fig. 5, the model was able to capture ELF PK of all mAbs reasonably well. The estimated model parameters

are shown in Table 5. The pinocytosis uptake for lung epithelial cells ($K_{upEpi}$) was estimated to be about tenfold higher than the uptake rate of endothelial cells, supporting faster clearance and shorter half-life of proteins in the ELF space. The upper airway rate of absorption ($Kabs_{UA}$) was estimated to be about 2000-fold higher than the alveolar rate of absorption ($Kabs_{al}$), the estimate suggests that the upper airway pathway has a faster $PS_{drug}$ process across ELF and interstitium as compared to alveolar and lower airway pathway.

### A priori model simulations

Figure 6 shows a priori simulated and observed concentration vs time profiles of VIS410 dosed intravenously at three dose levels, 15 mg/kg, 30 mg/kg and 50 mg/kg. Figure 7a, b shows the simulated and observed concentration vs time profiles of endogenous IgG and endogenous albumin levels at the steady state. The model performance for endogenous proteins was evaluated by comparing the steady-state concentration levels of these proteins to those published in the literature [30–32]. The SMAPE values of VIS410 at 15, 30 and 50 mg/kg were 90%, 55% and 68% respectively. Similarly, endogenous IgG simulations for Nasal Lavage fluid and BAL had a SMAPE value of 110% and 126% each. The SMAPE value for endogenous albumin levels in BAL was 4%. The simulations and the SMAPE values show that the model is overpredicting the endogenous IgG and VIS410 levels in the airways. In case of endogenous IgG levels in the airways, it is important to consider that the known variability in the endogenous plasma levels itself could one of the possible factors responsible for higher SMAPE values. Though the model is overpredicting endogenous IgG levels, endogenous levels of albumin have been captured well.

### Sensitivity analysis

In order to estimate the relative significance of the transport pathways involved, we performed local sensitivity analysis of four parameters: pinocytosis uptake rate of lung epithelial cells ($K_{upEpi}$, ), rate of protein absorption from upper airway ($Kabs_{UA}$) and lower airway ($Kabs_{LA}$), and FcRn concentrations in lung epithelial cells ($FcRn_{epi}$). The local sensitivity analysis of the four parameters as shown in Fig. 8. shows that FcRn concentration in pulmonary epithelial cells is the most sensitive parameter, followed by pinocytosis uptake of pulmonary epithelial cells. The rate of protein absorption in the upper airways was the next most sensitive parameter and the rate of protein absorption of the lower airways was found to be least sensitive.
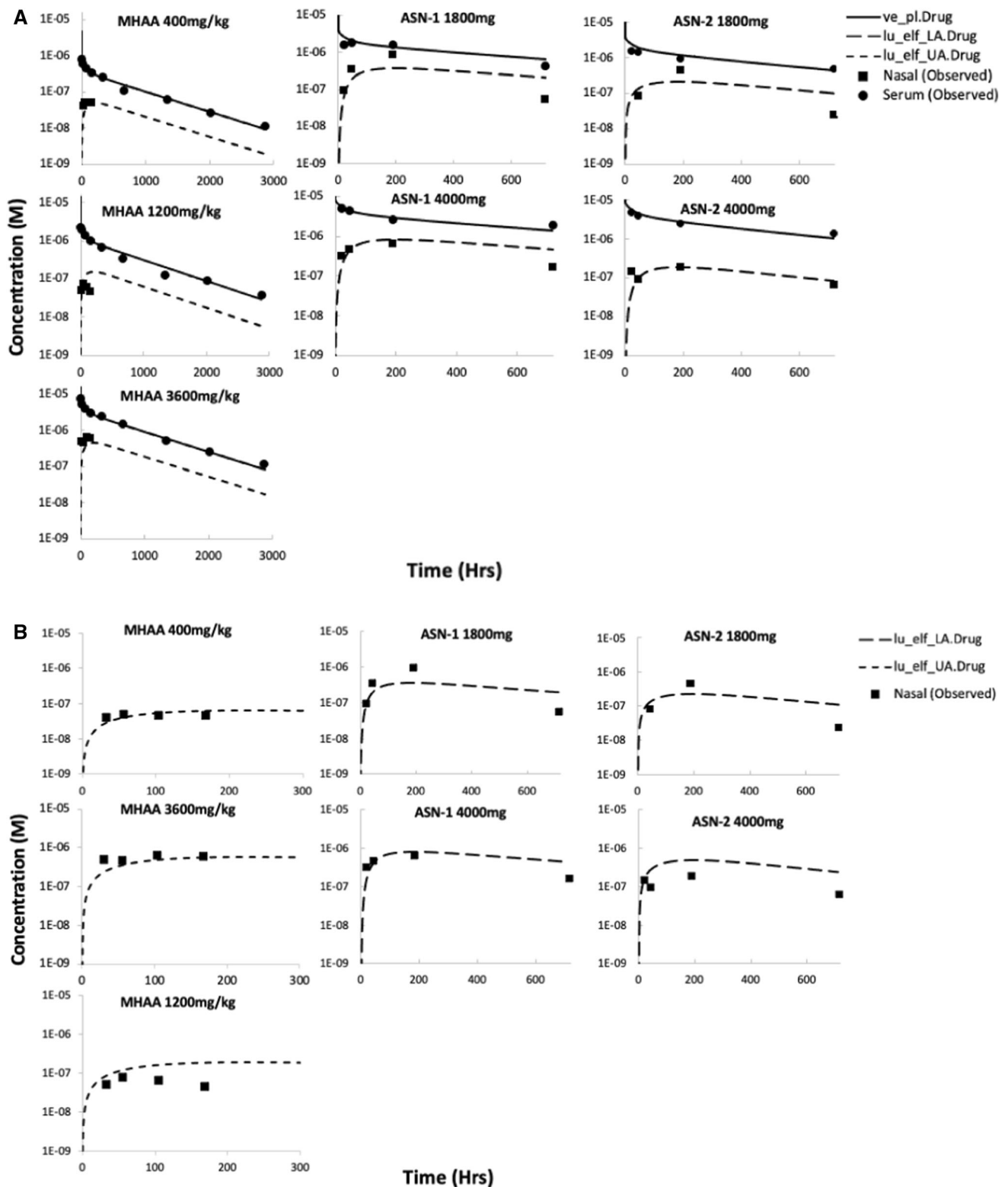
**Fig. 5 A** Observed (symbols) and fitted (lines) PK of intravenously administered mAbs in human subjects. MHAA (anti-influenza monoclonal antibody) was dosed IV at the dose levels of 400 mg, 1200 mg and 3600 mg, and nasal lavage PK (solid squares) was mapped to upper airway ELF concentrations. ASN-1 and ASN-2 (monoclonal antibodies) were dosed at 1800 mg and 4000 mg, and BAL PK (solid squares) was mapped to lower airway ELF concentrations. **B** Observed (symbols) and fitted (lines) ELF levels of MHAA, ASN-1 and ASN-2 during early time points

## Discussion

PBPK models aim to capture the physiological features of the organs in mathematical terms. Two-pore PBPK models help understand tissue distribution and clearance of proteins, and respective roles of filtration, diffusion and FcRn-mediated transcytosis in the disposition of proteins [37, 41–43]. As such, they can be expected to characterize not only the exogenously administered protein therapeutics but also endogenous proteins. This property makes PBPK models suitable for estimating the level of target engagement at the site-of-action and any downstream pharmacological effects (i.e., pharmacodynamics—PD) that may follow. With more than 15 monoclonal antibodies approved by the FDA for pulmonary indications, and more than 10 inhaled biologics in the preclinical stage of development for respiratory diseases [23], it is highly desirable to develop a PBPK model that can describe the disposition of biologics in the lungs and respiratory tract. In this manuscript we have expanded our previously published PBPK model [19] in this direction by including a more detailed lung compartment. In the first instance model focuses on lung exposure from systemic administration, but we expect it to be applicable in the opposite

**Table 5** Estimated parameter values and 90% confidence intervals

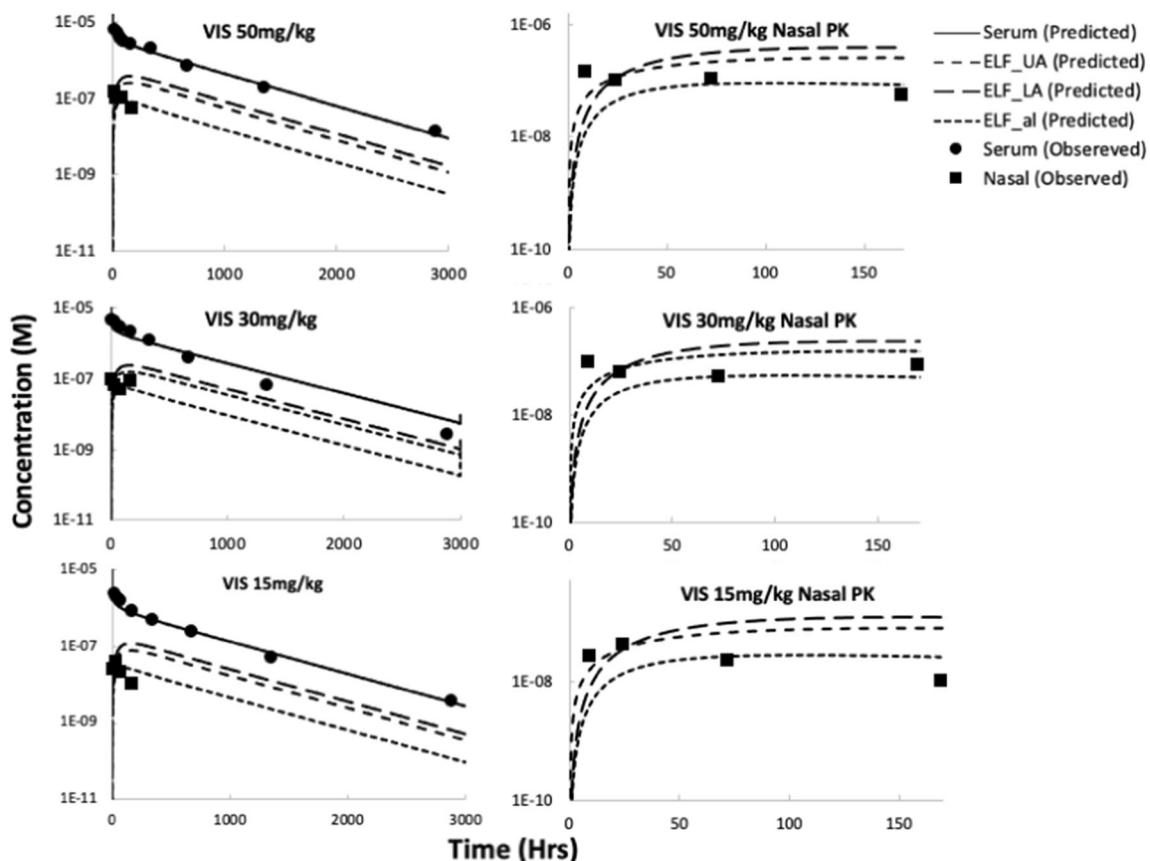| Parameter | Units | Value | Standard error | 95% Confidence intervals |
|---|---|---|---|---|
| $kdegV_{ASN1}$ | $1/h$ | 1.6E-4 | 4.7E-3 | 1E-5–1E-3 |
| $kdegV_{ASN2}$ | $1/h$ | 1E-3 | 5.7E-3 | 1E-4–5E-3 |
| $kdegV_{MHAA}$ | $1/h$ | 1E-5 | 3.6E-3 | 5E-6–1E-4 |
| $Kup_{epi}$ | $1/h$ | 1 | 0.1326 | 0.73–1.27 |
| $Kabs_{UA}$ | $1/h$ | 0.096 | 0.7589 | 0.01–0.4 |



**Fig. 6** Observed (Serum—circles, Nasal Lavage—Squares) and a priori simulated (lines) PK of exogenously administered antibody (VIS) that was dosed intravenously at 50 mg/kg, 30 mg/kg and 15 mg/kg doses

direction following pulmonary administration of proteins as well.

In the respiratory tract, the bronchi, the trachea and the nasal cavity connect the alveolar sacs to the atmosphere and aid in air filtration and act as channels for air flow [44]. The alveoli, the respiratory unit of the lungs is lined by two types of epithelial cells, type I and type II pneumocytes [45]. While the conducting passage way (nasal cavity, trachea, bronchi and the bronchioles) is lined up with pseudostratified columnar epithelial cells [46, 47], it does not contribute to the respiratory cycle [48]. In order to describe the complexity of airways in sufficient detail, we have modified our lung compartment by assuming the upper airways to be a part of this compartment. We have expanded the lung compartment into three areas: alveolar space, lower airway and upper airway. Physiologically the trachea, bronchi and the nasal cavity have a separate arterial blood flow, but for the sake of parsimony we have

assumed a common pulmonary flow for the whole upper airway compartment. As such, the total plasma flow to lungs was divided amongst alveolar pathway, upper airways, and lower airways as 92.5%, 5% and 2.5%, respectively.

The conducting passageways have evolved over time to develop an innate immune system to respond to constant threat of infection and inflammation. One such pathway include the mucociliary clearance systems [49]. The mucosal escalator pathway is present in the upper and lower airways of the pulmonary regions and is responsible for clearing the airway secretions. This clearance mechanism along with other clearance mechanism such as cough, peristalsis, two-phase gas–liquid flow and alveolar clearance are responsible for clearance of irritants or unwanted particles [50]. The rate of mucociliary clearance depends on the rate of movement of mucous across tracheal and bronchial epithelium, this rate of movement of mucous



**Fig. 7** Observed (red and blue lines) and a priori simulated (Black lines) levels of endogenous IgG and albumin. **A** endogenous IgG BAL levels (Blue line) and endogenous IgG Nasal Lavage concentrations (Red line). **B** Endogenous albumin BAL Levels (Red line) (Color figure online)
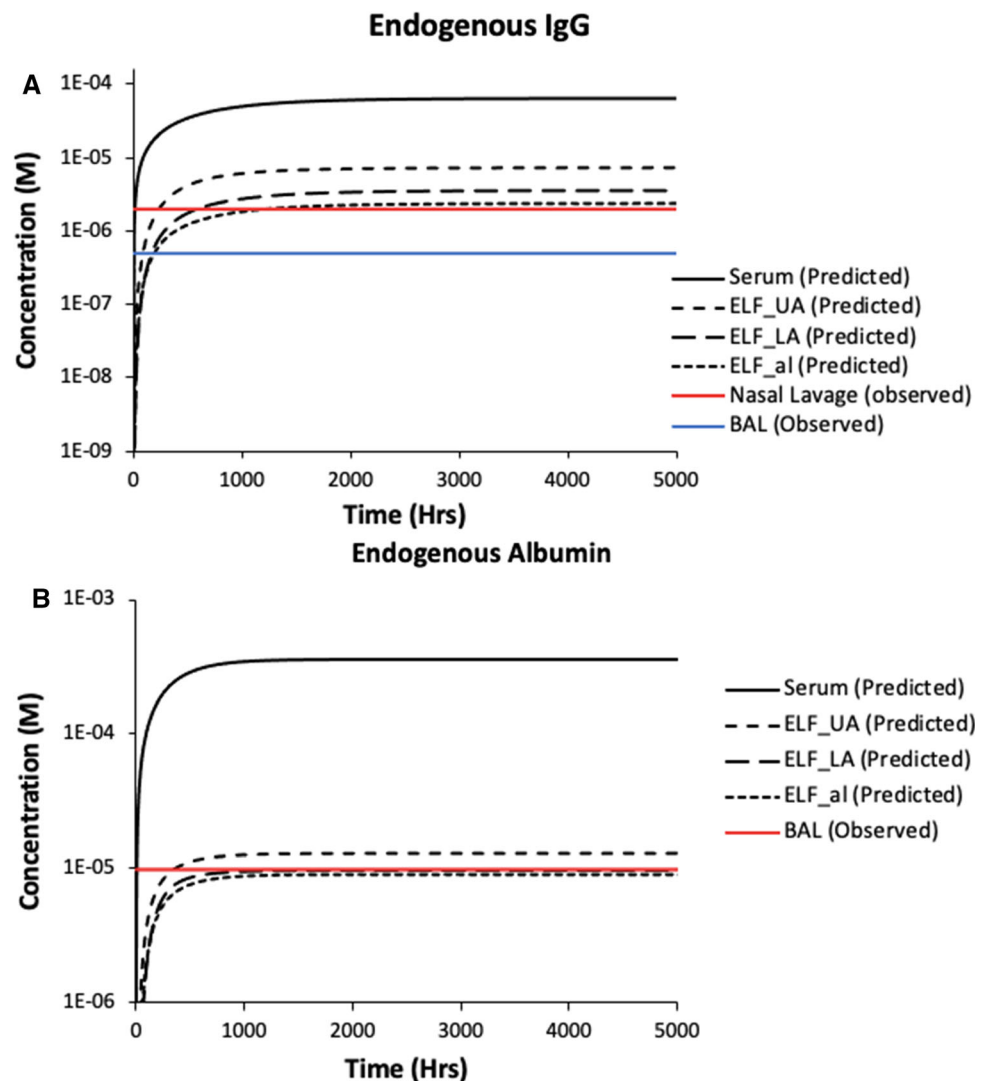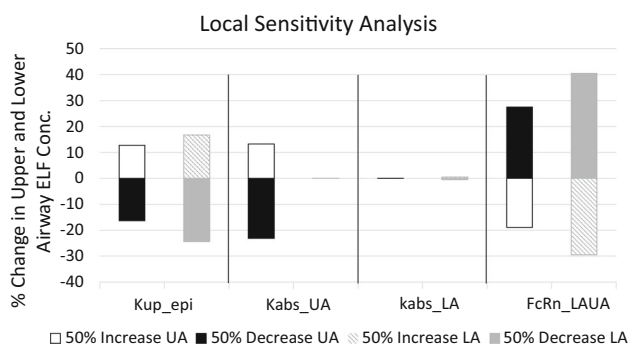
**Fig. 8** Local Sensitivity analysis of parameters related to upper and lower airway ELF concentration levels. The bar chart shows the percentage change in ELF_UA and ELF_LA AUCs with ± 50% alteration in model parameters. The higher the change in AUC the higher is the sensitivity of the parameter. Negative value of AUC represents decrease in the value

across the epithelium was reported by Smith, Gaffney et al. [51] to be 38.3 um/sec. This clearance rate is much slower than the clearance due to macrophages and not the dominant clearance mechanism in the epithelial lining fluid. Hence, for the sake of model simplicity all the clearance mechanism were pooled into one $K_{deg_{al}}$ term. This clearance rate as shown in Eq. 11 is derived from an empirical relation for the fraction of drug absorbed from the ELF ($F_{lu_{drug}}$) into systemic circulation, and thus takes all the clearance mechanisms in the ELF into account.

In order to estimate lung specific parameters, we utilized published data that investigated disposition of mAbs in pulmonary tissues. The default parameters of our platform PBPK model describe the plasma and tissue PK of a typical mAb, from which the behavior of any particular mAb can deviate to some extent. These differences were captured in the model for the mAbs studied by introducing arbitrary non-specific first-order clearance pathway in the plasma compartment which can mimic subtle mAb-dependent deviations, which can be related to changes in interaction with FcRn [52], non-specific binding to the cell surface etc. [53]. Once the mAb PK-specific features were captured, we used three datasets for fitting the two global lung compartment parameters, and a priori simulated pulmonary PK of a validation mAb as well as endogenous IgG and albumin. Good agreement between model simulated and observed pulmonary concentrations of externally administered mAbs and endogenous proteins indicates that the pulmonary transport and clearance mechanisms were captured well by the PBPK model. In addition, the PBPK model helped in understanding the rate of certain physiological processes such as the rate of non-specific degradation of proteins in ELF. The model suggests that this process can be significant [9], and our calculations suggest that the half-life of a mAb in alveolar ELF is very short

(few hours) and close to that estimated for smaller proteins like insulin [9].

The average half life of IgG1 in humans is about 21 days, however in case of VIS410 antibody the half life is just 12 days. Consequently, the plasma PK for VIS410 antibody was captured by estimating the non-specific clearance term ($kdegV_{VIS410}$) in vascular space of the model. This relatively short half-life of VIS410 indicates presence of unknown molecule or target dependent elimination process for this mAb. Nontheless, after adjusting the plasma PK, the data was used as an validation dataset. The model was able to predcit ELF concentrations of VIS410 reasonably well (Fig. 6), albeit there is some overestimation of ELF concentrations and SMAPE value was found to be > 33%.

The SMAPE value, which represents the levels of over and underprediction by the model is higher than 33% (more than two-fold over or underpredicted) for VIS410 mAb and endogenous IgG levels in pulmonary tissues. It is important to note that experimental measurements of ELF concentrations are very challenging due to the small volumes and vanishing thickness of the fluid film on the surface of the cells. BAL is commonly used as a surrogate but carries with it the uncertainty of significant dilution to an unknown extent. The dilution factor is commonly calculated from the endogenous urea concentration, but it carries a known systematic deviation due to rapid influx of systemic urea during the recovery step, the extent of which depends on the duration of the procedure [54]. As a result, the dilution estimates carry significant degree of uncertainty. Nonetheless, all of the endogenous and exogenous data except endogenous IgG data used for our lung PBPK model fitting and simulation was urea normalized to get a representation of true ELF concentrations of dosed and endogenous proteins. Yet, there is still a significant levels of uncertainty in urea normalized concentration, which possibly could be responsible for higher SMAPE values.

The sensitivity analysis as shown in Fig. 8, shows that FcRn concentration is the most sensitive parameter, followed by pinocytosis uptake, followed by rate of protein absorption in the upper airways. The rate of protein absorption in the lower airways was not a very sensitive parameter. Though, FcRn concentration is the most sensitive parameter, there is varying data on the FcRn expression levels in alveolar and bronchial tissues. Different papers show different degree of staining in alveolar, bronchial and nasal tissues in humans [25, 26, 55]. In the absence of quantifiable data we have assumed the FcRn concentration to be the same in all the three lung compartments. Since, rate of protein absorption from lower airway ($Kabs_{LA}$) was not found to be a very sensitive parameter, this parameter was fixed to mimic the rate of protein absorption from the alveolar pathway. The value

for pinocytosis uptake of proteins by lung epithelial cells ($K_{upEpi}$) was estimated with good confidence, but the standard error (as seen by large confidence interval) for the rate of protein absorption parameter in upper airway compartment ($Kabs_{UA}$) was high, which warrants further in-vivo or in-vitro experiments to validate this parameter value.

The relative importance of FcRn-mediated and paracellular transport has been the subject of intense research, with the conclusion that FcRn only contributes significantly to alveolar exchange at very low IgG concentrations and relatively little at physiological levels [22]. Our model suggests that the FcRn concentration in endosomal space is a very sensitive parameter. Hence, FcRn meditated transcytosis might actually be an important pathway. However, the fact that there is little to no difference between the plasma/ELF ratios of IgG1, IgG2, IgG3 and IgG4 in humans [31] despite significant differences in half-lives and affinities for FcRn hints otherwise. Likewise, no statistically significant difference was found between the BAL:plasma ratios for wild-type and half-life extended YTE-variants of MEDI-524 with enhanced affinity for FcRn [5], which was interpreted as evidence of the negligible role played by FcRn-mediated transcytosis in the mAb exchange between lung interstitium and ELF. Since sensitivity analysis was done by calculating the percentage change in AUCs with ± 50% alteration in model parameters, the default parameter value would have a significant effect on the sensitivity of the parameter. Thus, it is important to stress the need to quantify absolute or relative FcRn concentration levels in lung epithelial cells. There is a possibility that the relative contribution of FcRn-mediated transport and diffusion across the epithelium might differ in different regions of the respiratory pathway depending on the expression levels of FcRn and the thickness of epithelial lining fluid in the corresponding region. In the absence of reports about relative FcRn concentration levels in these different regions of the pulmonary pathway we could only speculate which transport mechanism is more important.

Following a priori simulations of the model, it was found that the model was able to capture the observed data well except the endogenous IgG levels. The model overpredicted the endogenous IgG level, the over predication of upper airway ELF concentration is about 4 folds higher than the reported Nasal Lavage concentration reported by Yoshida et al. [30] The lower airway ELF concentration is about tenfold higher than the BAL concentration reported by Merrill et al. [31] It is possible that this might be due to the fact that this data is not urea normalized. The predicted average IgG concentration gradient between plasma and ELF predicted by our model is close to the tenfold difference for a number of mAbs measured in monkeys [56].

The PBPK model proposed here can predicit the pulmonary disposition of systemically administered mAbs resonably well, amd it supports the hypothesis that regions of the lungs that are not involved in gas exchange also participate in absorption of drugs due to FcRn transcytosis and permeabilty of drugs across the epithelial cell membrane. However, although the pulmonary dosing pathway can be modelled in the presented framework, the model is still not validated to predict systemic exposure of inhaled proteins, and thus we need to further look into quantifying the absorption and systemic exposure of proteins observed following that route of administration.

In summary, here we have presented a novel PBPK model to characterize lung disposition of protein therapeutics in humans. Our lung PBPK model successfully predicts exogenous mAb levels in epithelial lining fluid after systemic administration of mAbs. Further our model also captures the endogenous IgG and albumin levels in ELF. This model will aid in the prediction of local lung concentration for systemically administered proteins and help assess the potential of new therapies targeted for pulmonary diseases. Furthermore, the model can be easily supplemented with target molecule(s) of interest to estimate the pharmacology at the site-of-action and can be adapted to account for the effect of pathophysiology on lung PK of protein therapeutics.

## Declarations

## References

1. Soriano JB et al (2020) Prevalence and attributable health burden of chronic respiratory diseases, 1990–2017: a systematic analysis for the global burden of disease study 2017. Lancet Respir Med 8(6):585–596

2. Ferkol T, Schraufnagel D (2014) The global burden of respiratory disease. Ann Am Thorac Soc 11(3):404–406

3. Syamlal G, Bhattacharya A, Dodd KE (2020) Medical expenditures attributed to asthma and chronic obstructive pulmonary disease among workers—United States, 2011–2015. Morb Mortal Wkly Rep 69(26):809

4. Leader B, Baca QJ, Golan DE (2008) Protein therapeutics: a summary and pharmacological classification. Nat Rev Drug Discovery 7(1):21–39

5. Dall'Acqua WF, Kiener PA, Wu H (2006) Properties of human IgG1s engineered for enhanced binding to the neonatal Fc receptor (FcRn). J Biol Chem 281(33):23514–23524

6. Itoga NK et al (2014) Mechanical factors affecting nebulized albuterol aerosol particle sizes for asthma drug delivery. Am J Emerg Med 32(6):569–572

7. Heyder J (2004) Deposition of inhaled particles in the human respiratory tract and consequences for regional targeting in respiratory drug delivery. Proc Am Thorac Soc 1(4):315–320

8. Franciosi L et al (2013) Proteomic analysis of human epithelial lining fluid by microfluidics-based nanoLC-MS/MS: a feasibility study. Electrophoresis 34(18):2683–2694

9. Sakagami M (2013) Systemic delivery of biotherapeutics through the lung: opportunities and challenges for improved lung absorption. Ther Deliv 4(12):1511–1525

10. Derom E, Thorsson L (2002) Factors affecting the clinical outcome of aerosol therapy. Drug delivery to the lung. Marcel Dekker Inc, New York, pp 143–171

11. Dumont JA et al (2005) Delivery of an erythropoietin-Fc fusion protein by inhalation in humans through an immunoglobulin transport pathway. J Aerosol Med 18(3):294–303

12. Kim D et al (2003) Dose-response relationships of inhaled insulin delivered via the Aerodose insulin inhaler and subcutaneously injected insulin in patients with type 2 diabetes. Diabetes Care 26(10):2842–2847

13. Buttini MF, Probst MSE, Valdelatas AM (2013) Inhalable therapeutic biologics a paradigm shift for non-invasive efficient medical treatments. Biotechnology 2011(2012):2014

14. Borghardt JM et al (2016) Model-based evaluation of pulmonary pharmacokinetics in asthmatic and COPD patients after oral olodaterol inhalation. Br J Clin Pharmacol 82(3):739–753

15. Gaohua L et al (2015) Development of a multicompartment permeability-limited lung PBPK model and its application in predicting pulmonary pharmacokinetics of antituberculosis drugs. CPT: Pharma Syst Pharmacol 4(10):605–613

16. Hendrickx R et al (2018) Translational model to predict pulmonary pharmacokinetics and efficacy in man for inhaled bronchodilators. CPT Pharma Syst Pharmacol 7(3):147–157

17. Shao J, Wang Y, Hochhaus G (2021) Semi-mechanistic PK/PD model to assess pulmonary targeting of beclomethasone dipropionate and its active metabolite. Eur J Pharm Sci 159:105699

18. Morgan P et al (2012) Can the flow of medicines be improved? Fundamental pharmacokinetic and pharmacological principles toward improving Phase II survival. Drug Discovery Today 17(9–10):419–424

19. Sepp A et al (2019) Computer-assembled cross-species/cross-modalities two-pore physiologically based pharmacokinetic model for biologics in mice and rats. J Pharmacokinet Pharmacodyn 46(4):339–359

20. Shah DK, Betts AM (2012) Towards a platform PBPK model to characterize the plasma and tissue disposition of monoclonal antibodies in preclinical species and human. J Pharmacokinet Pharmacodyn 39(1):67–86

21. Bitonti AJ, Dumont JA (2006) Pulmonary administration of therapeutic proteins using an immunoglobulin transport pathway. Adv Drug Deliv Rev 58(9–10):1106–1118

22. Hastings RH, Folkesson HG, Matthay MA (2004) Mecanisms of alveolar protein clearance in the intact lung. Am J Physiol Lung Cell Mol Physiol 286(4):L679–L689

23. Liang W et al (2020) Pulmonary delivery of biological drugs. Pharmaceutics 12(11):1025

24. Kim K-J et al (2004) Net absorption of IgG via FcRn-mediated transcytosis across rat alveolar epithelial cell monolayers. Am J Physiol Lung Cell Mol Physiol 287(3):L616–L622

25. Bequignon E et al (2019) FcRn-dependent transcytosis of monoclonal antibody in human nasal epithelial cells in vitro: a prerequisite for a new delivery route for therapy? Int J Mol Sci 20(6):1379

26. Spiekermann GM et al (2002) Receptor-mediated immunoglobulin G transport across mucosal barriers in adult life: functional expression of FcRn in the mammalian lung. J Exp Med 196(3):303–310

27. Magyarics Z et al (2019) Randomized, double-blind, placebo-controlled, single-ascending-dose study of the penetration of a monoclonal antibody combination (ASN100) targeting staphylococcus aureus cytotoxins in the lung epithelial lining fluid of healthy volunteers. Antimicrob Agents Chemother. https://doi.org/10.1128/AAC.00350-19

28. Deng R et al (2018) Pharmacokinetics of MHAA4549A, an anti-influenza a monoclonal antibody, in healthy subjects challenged with influenza a virus in a phase IIa randomized trial. Clin Pharmacokinet 57(3):367–377

29. Wollacott AM et al (2016) Safety and upper respiratory pharmacokinetics of the hemagglutinin stalk-binding antibody VIS410 support treatment and prophylaxis based on population modeling of seasonal influenza a outbreaks. EBioMedicine 5:147–155

30. Yoshida T et al (2005) A quantitative analysis of cedar pollen-specific immunoglobulins in nasal lavage supported the local production of specific IgE, not of specific IgG. Microbiol Immunol 49(6):529–534

31. Merrill WW et al (1985) Immunoglobulin G subclass proteins in serum and lavage fluid of normal subjects. Quantitation and comparison with immunoglobulins A and E. Am Rev Respir Dis 131(4):584–587

32. Wilson DR et al (2002) Increases in allergen-specific IgE in BAL after segmental allergen challenge in atopic asthmatics. Am J Respir Crit Care Med 165(1):22–26

33. Wiig H, Swartz MA (2012) Interstitial fluid and lymph formation and transport: physiological regulation and roles in inflammation and cancer. Physiol Rev 92(3):1005–1060

34. Garg A, Balthasar JP (2007) Physiologically-based pharmacokinetic (PBPK) model to predict IgG tissue kinetics in wild-type and FcRn-knockout mice. J Pharmacokinet Pharmacodyn 34(5):687–709

35. Urva SR, Yang VC, Balthasar JP (2010) Physiologically based pharmacokinetic model for T84.66: a monoclonal anti-CEA antibody. J Pharm Sci 99(3):1582–1600

36. Abdiche YN et al (2015) The neonatal Fc receptor (FcRn) binds independently to both sites of the IgG homodimer with identical affinity In MAbs. Taylor & Francis

37. Sepp A, Bergstrom M, Davies M (2020) Cross-species/cross-modality physiologically based pharmacokinetics for biologics: 89Zr-labelled albumin-binding domain antibody GSK3128349 in humans. MAbs 12(1):1832861

38. Fröhlich E et al (2016) Measurements of deposition, lung surface area and lung fluid for simulation of inhaled compounds. Front Pharmacol 7:181–181

39. Ménache MG et al (1997) Upper respiratory tract surface areas and volumes of laboratory animals and humans: considerations for dosimetry models. J Toxicol Environ Health 50(5):475–506

40. Mercer RR et al (1994) Cell number and distribution in human and rat airways. Am J Respir Cell Mol Biol 10(6):613–624

41. Davda JP et al (2008) A physiologically based pharmacokinetic (PBPK) model to characterize and predict the disposition of monoclonal antibody CC49 and its single chain Fv constructs. Int Immunopharmacol 8(3):401–413

42. Li Z, Shah DK (2019) Two-pore physiologically based pharmacokinetic model with de novo derived parameters for predicting plasma PK of different size protein therapeutics. J Pharmacokinet Pharmacodyn 46(3):305–318

43. Sepp A et al (2015) Development of a physiologically based pharmacokinetic model for a domain antibody in mice using the two-pore theory. J Pharmacokinet Pharmacodyn 42(2):97–109

44. Cotes JE, Chinn DJ, Miller MR (2009) Lung function: physiology, measurement and application in medicine. John Wiley & Sons

45. Guillot L et al (2013) Alveolar epithelial cells: master regulators of lung homeostasis. Int J Biochem Cell Biol 45(11):2568–2573

46. Otto W (2002) Lung epithelial stem cells. J Pathol 197(4):527–535
47. Plopper CG (1983) Comparative morphologic features of bronchiolar epithelial cells: the Clara cell. Am Rev Respir Dis 128:S37–S41
48. Comroe JH (1966) The lung. Sci Am 214(2):56–71
49. Wanner A, Salathé M, O'Riordan TG (1996) Mucociliary clearance in the airways. Am J Respir Crit Care Med 154(6):1868–1902
50. Houtmeyers E et al (1999) Regulation of mucociliary clearance in health and disease. Eur Respir J 13(5):1177–1188
51. Smith DJ, Gaffney EA, Blake JR (2008) Modelling mucociliary clearance. Respir Physiol Neurobiol 163(1–3):178–188
52. Jensen PF et al (2017) A two-pronged binding mechanism of IgG to the neonatal Fc receptor controls complex stability and IgG serum half-life. Mol Cell Proteom 16:451
53. Liu S et al (2021) Effect of variable domain charge on in vitro and in vivo disposition of monoclonal antibodies in Mabs. Taylor & Francis
54. Kipnis E (2005) Using urea as an endogenous marker of bronchoalveolar lavage dilution. Crit Care Med 33(9):2153
55. Heidl S et al (2016) Localization of the human neonatal Fc receptor (FcRn) in human nasal epithelium. Protoplasma 253(6):1557–1564
56. Spiess C, Zhai Q, Carter PJ (2015) Alternative molecular formats and therapeutic applications for bispecific antibodies. Mol Immunol 67:95–106